Scripta Materialia 273 (2026) 117106

Contents lists available at ScienceDirect

Scripta Materialia

journal homepage: www.journals.elsevier.com/scripta-materialia

Pressure-induced phase transitions of amorphous silicon nanoparticles

Haotian Zhu [a,1], Shuai Liu [a,1], Di Peng [a,b], Fujun Lan [a,b,c], Yuxin Liu [a], Guangrun Zhong [a], Hongbo Lou [a,b], Qiaoshi Zeng [a,b,*], Zhidan Zeng [a,*]

[a] Center for High Pressure Science and Technology Advanced Research (HPSTAR), Shanghai 201203, China
[b] Shanghai Key Laboratory of Material Frontiers Research in Extreme Environments (MFree), Shanghai Advanced Research in Physical Sciences (SHARPS), Shanghai 201203, China
[c] Shanghai Institute of Laser Plasma, Shanghai 201800, China

ARTICLE INFO

Keywords:
Amorphous silicon
Nanoparticles
High pressure
Phase transition
Synchrotron x-ray diffraction

ABSTRACT

Amorphous silicon (a-Si) plays a significant role in various modern technologies. Therefore, understanding its stability is of both fundamental and technological importance. While pressure-induced phase transitions in a-Si have been extensively studied, the effect of domain size remains unclear. In this study, we synthesized amorphous silicon nanoparticles (a-SiNPs) with an average size of ~9 nm and investigated their pressure-induced phase transitions using *in situ* high-pressure Raman spectroscopy and synchrotron X-ray diffraction. These results reveal that a-SiNPs transform into β-Sn phase at ~10.8 GPa, rather than a previously reported high-density amorphous phase. Upon decompression, the β-Sn phase reverts to a-Si. The phase transition pathway and transition pressure are similar to those observed in bulk a-Si, indicating that domain size is not a determining factor for inducing polyamorphism in a-Si. These findings bring new insights into the thermodynamics and kinetics of phase transitions in a-SiNPs and provide experimental constraints for theoretical studies of a-Si.

Amorphous silicon (a-Si) plays a crucial role in both applied and fundamental research. In practical applications, a-Si is widely used in thin-film transistors, solar cells, displays, flexible electronics, and photodetectors [1,2]. In fundamental research, as an elemental amorphous material, a-Si serves as an important model system for understanding amorphous materials [3,4]. A-Si can be synthesized using various methods, including chemical vapor deposition, self-ion implantation, solid-state metathesis [1,5,6]. Although the local structure of a-Si may vary slightly depending on synthesis methods, they all feature a disordered, tetrahedrally coordinated network structure with an average coordination number close to four. As a thermodynamically metastable material, the stability of a-Si is of particular interest and importance.

One of the most intriguing transitions in a-Si is the pressure-induce polyamorphic transition from low-density amorphous (LDA) to high-density amorphous (HDA), which might be associated with high-density liquid Si and has attracted broad research interest since its experimental discovery two decades ago [6,7]. Various theoretical studies have confirmed this kind of pressure-induced LDA-HDA transition in a-Si characterized by a significant volume collapse and an increase in average coordination number. However, different studies have proposed diverse transition pressures and mechanisms [6,8–11]. In addition, among the extensive experimental research, results remain surprisingly inconsistent and controversial [6,12–17] *E.g.*, the polyamorphic transition in a-Si was first reported in a high-pressure Raman study on porous Si with nanometer-scale domains, in which porous crystalline Si (c-Si) transformed into HDA when compressed above 10 GPa, and HDA transformed into LDA upon decompression [7]. Later, a study on solid-state metathesis synthesized a-Si found its optical properties and resistance changed abruptly between 14.2–15.7 GPa and 10–12 GPa, which is consistent with an LDA-HDA transition [6]. Further high-pressure pair distribution function (PDF) study on the same a-Si sample suggests that the first peak in S(q) shifted to larger q values at 13.5 GPa, providing structural evidence on the LDA-HDA transition [13]. High-pressure Raman study on a-Si thin films synthesized via plasma-enhanced chemical vapor deposition also reported a LDA-HDA transition [15]. In contrast, high-pressure X-ray diffraction (XRD) studies on a-Si synthesized by magnetron-sputtering found it directly transforms to the β-Sn phase (Si-II) at 12.1 GPa [14]. High-pressure XRD studies on bulk a-Si also found transitions to Si-II at 10.0 GPa [12] or to the rhombohedral phase (Si-XII) and Si-II at 9.8 GPa [17]. These

* Correspondence author.
E-mail addresses: zengqs@hpstar.ac.cn (Q. Zeng), zengzd@hpstar.ac.cn (Z. Zeng).
[1] These authors contributed equally to this work

https://doi.org/10.1016/j.scriptamat.2025.117106
Received 7 May 2025; Received in revised form 4 November 2025; Accepted 13 November 2025
Available online 21 November 2025

discrepancies have been partially attributed to impurity in a-Si in a recent study [14]. It should be noted that domain size effect may also play an important role, as some prior studies used nanostructured a-Si, [7,15] while others used bulk samples [12,14,17].

It is well-recognized that many nanostructured materials exhibit pressure-induced phase transitions that significantly differ from those of their bulk counterparts. Taking crystalline silicon (c-Si) for example, bulk c-Si samples typically transform from the diamond cubic phase (Si-I) to the metallic Si-II at ~12 GPa, then to the Imma phase (Si-XI) at ~13.2 GPa and the primitive hexagonal phase (Si-V) at ~16 GPa [18]. However, in nanostructured Si, the phase transition pathway shifts to Si-I →Si-XI or Si-I →Si-V as domain size decreases, bypassing the Si-II and Si-XI phases [19–21]. Additionally, the critical transition pressure in Si nanoparticles (SiNPs) and Si nanowires increases substantially compared with that in bulk silicon [20,22]. For instance, the transition pressures in SiNPs (Si-I) were reported to be 15.6 GPa (~3 nm), 16.4 GPa (~9 nm), 16.9 GPa (~18 nm), 22 GPa (~10 nm), and 17–22 GPa (3.2–4.5 nm) [20,21,23–25]. However, whether amorphous SiNPs (a-SiNPs) exhibit distinct phase transition pathways or pressures compared to bulk a-Si, namely, an obvious size effect, remains unclear.

In this study, we synthesized ~9 nm a-SiNPs and investigated their pressure-induced phase transitions using both *in situ* high-pressure synchrotron XRD and Raman spectroscopy. The phase transition pathway and transition pressure of the a-SiNPs were compared with those of bulk a-Si and crystalline SiNPs. The results suggest that phase transitions in a-Si are similar to the bulk c-Si and are not significantly affected by domain size. These findings could help deepen our understanding of stability and phase transitions in a-Si.

Crystalline SiNPs with an average particle size of ~9 nm were synthesized by thermal decomposition of silicon monoxide at 1000 °C in an argon-protected atmosphere [19]. The SiNPs, along with several ruby spheres, were loaded into a ~200 μm hole drilled in a pre-indented rhenium gasket of a 400 μm-culet diamond anvil cell (DAC). The sample was compressed to ~24 GPa and held at that pressure for 24 h before decompression. A-SiNPs were obtained after pressure release. Both the as-synthesized SiNPs and the a-SiNPs recovered from high pressure were characterized by transmission electron microscopy (FEI, Tecnai F20 S-Twin TEM).

High-pressure Raman spectra were collected in a backscattering geometry using a 488 nm excitation laser, a 1800 g/mm grating, and a $\alpha \times$ 10 objective lens. To minimize laser-induced heating, the laser power was limited to 5 mW. Because the Raman signal of a-Si and high-pressure Si phases such as Si-II are weak, each spectrum was acquired with a collection time of 5 min. Type IIa diamond anvils with ultra-low luminescence were used to reduce background signals from anvils. The sample chamber was a 150 μm diameter hole drilled in a pre-indented rhenium gasket within a 400 μm-culet DAC, with argon serving as the pressure-transmitting medium. Pressure was determined using the R1 fluorescence line of ruby.

For high-pressure XRD experiments, a-SiNPs were loaded into a symmetric DAC along with tiny ruby spheres and a gold foil. Pressure was determined using the equation of state of gold [26]. The sample chamber was a 200 μm diameter hole drilled in a pre-indented rhenium gasket of a 400 μm-culet DAC, with helium as the pressure-transmitting medium. *In situ* high-pressure angle-dispersive XRD experiments were conducted at beamline 15U1 of Shanghai Synchrotron Radiation Facility (SSRF) using a focused X-ray beam with a wavelength of 0.6199 Å. Background scattering from the high-pressure environment was collected by shining X-ray beam through the pressure medium beside the sample and subtracted to obtain diffraction signal from the sample. A MAR165 charge-coupled device (CCD) detector was used for data collection, and the two-dimensional images were integrated into XRD patterns using Dioptas software [27].

Fig. 1 shows the transmission electron microscopy (TEM) images and selected area electron diffraction (SAED) patterns of the initial crystalline SiNPs and the sample recovered from ~24 GPa. The TEM image confirms an average particle size of ~9 nm, consistent with previous report [19,20]. The diffuse scattering halo in the SAED pattern of the high pressure recovered sample confirms that it is fully amorphous. Additionally, Raman spectra recorded during the compression-decompression cycle show that the high-pressure Si-II phase transforms to an amorphous phase upon decompression (see Fig. S1). These results indicate that a-SiNPs can be obtained through pressure-induced phase transitions, in agreement with previous findings [20].

To investigate pressure-induced phase transitions in a-SiNPs, we conducted *in situ* high-pressure Raman spectroscopy up to 24.0 GPa. As shown in Fig. 2a, the Raman spectrum of a-SiNPs exhibits two broad bands centered at 100–200 and 450–550 cm^{-1}, corresponding to the transverse-acoustic (TA) and transverse-optical (TO) vibrational modes of a-Si, respectively. During compression, the TO band of a-Si weakens at 10.5 GPa. At 12.5 GPa, a new peak emerges near 120 cm^{-1}, corresponding to the longitudinal-optical (LO) mode of the Si-II phase [28,29], indicating a phase transition from a-Si to Si-II. The TA and TO peaks of a-Si fully disappear at 13.5 GPa, confirming the complete transformation to Si-II. Meanwhile, the broad Raman band near 400 cm^{-1} attributed to HDA Si is not visible, implying the absence of a polyamorphic transition. The optical properties of the sample change with the phase transition. As shown in Fig. 3, the thinner regions of the sample appear translucent with a brownish color, consistent with the

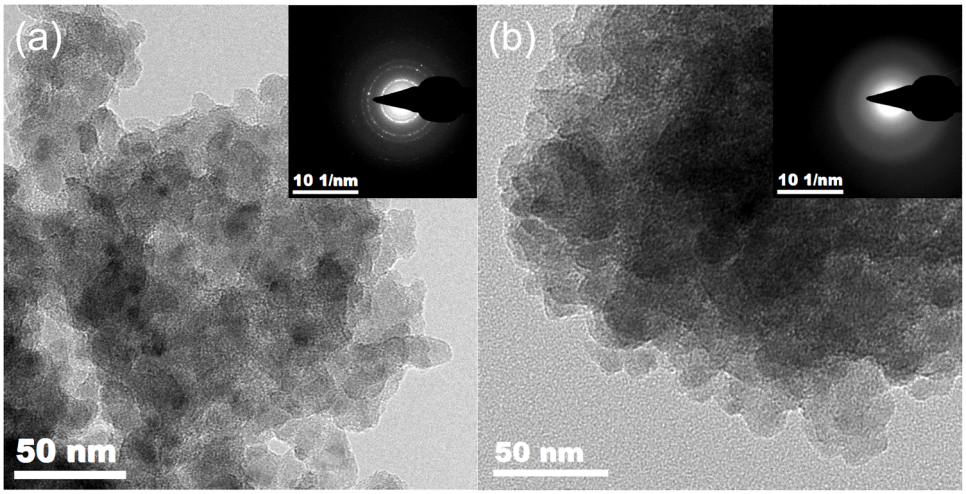

Fig. 1. TEM images of the initial crystalline SiNPs (a) and the a-SiNPs sample recovered from ~24 GPa (b). The insets show their corresponding SAED patterns.

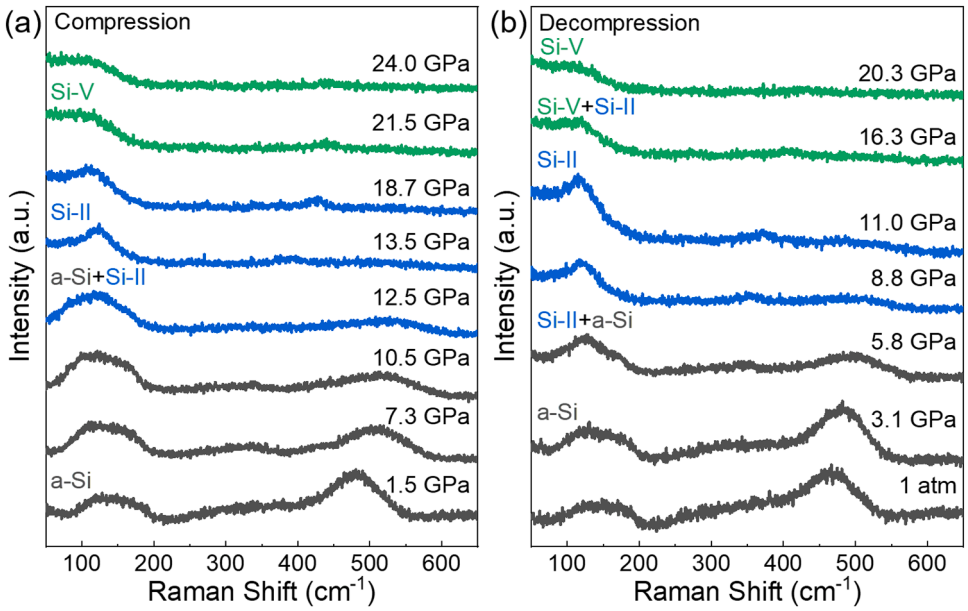

Fig. 2. In situ high-pressure Raman spectra of a-SiNPs at selected pressures during compression up to 24.0 GPa (a) and decompression (b). Argon was used as the pressure-transmitting medium.

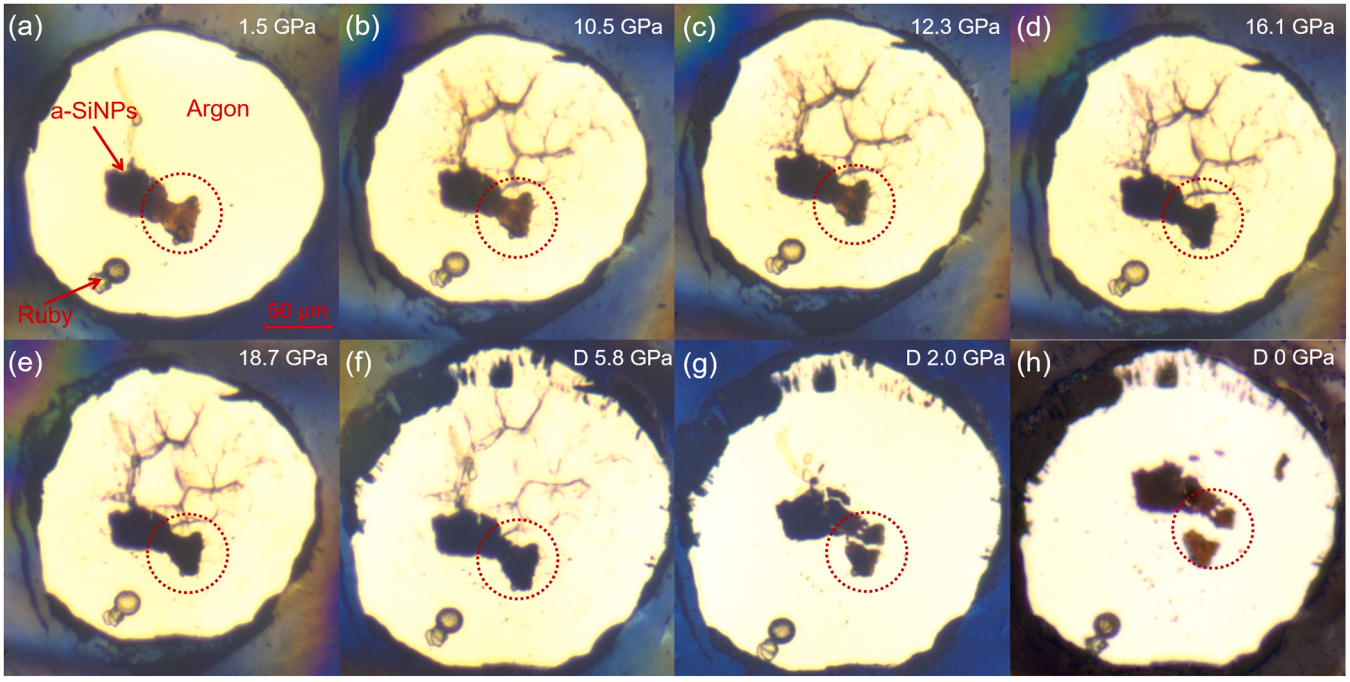

Fig. 3. (a)-(h) Optical microscope images of the a-SiNPs sample for the high-pressure Raman experiment at selected pressures upon compression and decompression. The applied pressures are indicated in each panel. The translucent region of the sample is indicated by a dashed circle.

optical bandgap of ~1.7 eV for a-Si [30]. During compression, some areas of the sample become less translucent at 12.3 GPa and eventually turn opaque at 16.1 GPa, aligning with the metallic nature of Si-II. With further compression, the LO peak of Si-II at ~120 cm^{-1} disappears at ~21.5 GPa, marking the transition to the simple hexagonal phase (Si-V). Upon decompression (see Fig. 2b), it reverts to Si-II at ~11.0 GPa, followed by a transition back to a-Si at 5.8 GPa. Correspondingly, the sample regains translucency after pressure release.

Due to the weak Raman signal of the high-pressure phases, we carried out *in situ* high-pressure XRD experiments to investigate the structural transitions further. As shown in Fig. 4a, both the first and second diffraction peaks of a-Si shift continuously toward higher q values during compression. However, no sudden shift in the first diffraction peak, which would indicate a polyamorphic transition [14], is observed, suggesting the absence of such a transition. At approximately 10.8 GPa, sharp crystalline diffraction peaks emerge, which can be identified as Si-II. This phase transition pressure is slightly lower than that determined by Raman spectroscopy, probably due to the higher sensitivity of XRD than Raman in terms of Si-II whose Raman signal is quite weak. As pressure increases, the intensity of Si-II peaks rises at the expense of a-Si peaks. With further compression, Si-II transforms into Si-XI at 18.3 GPa and subsequently into Si-V at 21.7 GPa. The phase identification was

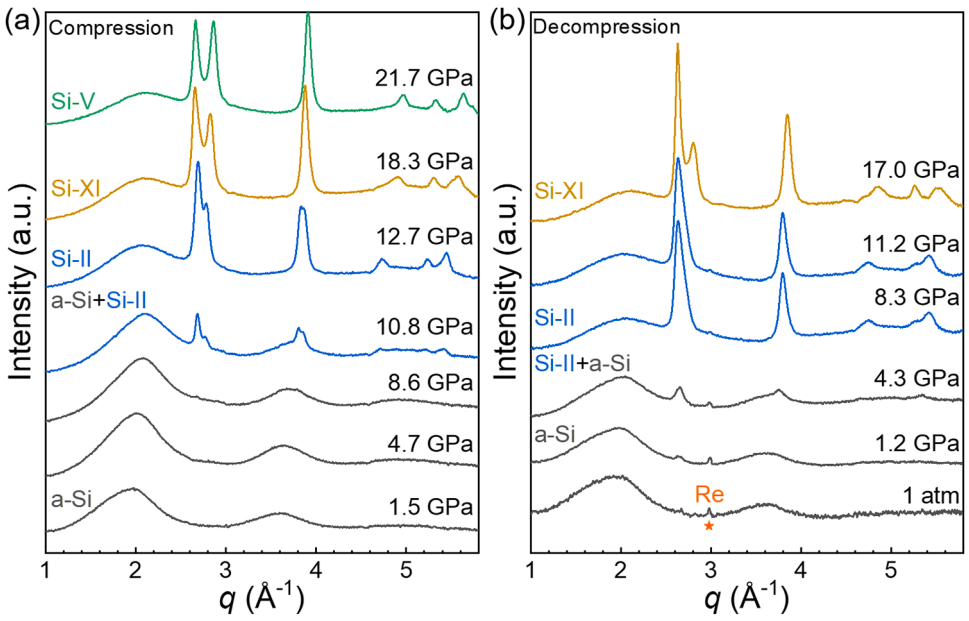

Fig. 4. In situ high-pressure XRD patterns of a-SiNPs during compression up to 21.7 GPa (a) and decompression (b). The X-ray wavelength was 0.6199 Å. Helium was used as the pressure-transmitting medium.

verified by comparing Rietveld refinement results using different phase structures (Si-II, Si-XI, and Si-V). These phase transitions are reversible upon decompression, with Si-II reverting to a-Si at 4.3 GPa (see Fig. 4b), consistent with Raman results. The Si-II-to-a-Si transition upon decompression observed in XRD and Raman experiments is in line with the previous studies on nanostructured Si [20,21].

Our experimental results indicate that ~9 nm a-SiNPs transform into Si-II at 10.8 GPa, rather than an HDA phase. This phase transition pathway aligns with that observed in high-purity a-Si thin films (~5 μm thick) and in bulk a-Si, which transform into Si-II phase at 12.1 GPa or 10 GPa [12,14]. The consistent phase transition pathway and similar transition pressures suggest that the pressure-induced phase transitions in a-Si are not significantly affected by domain size. This is quite different from the case in c-Si, where phase transitions strongly depend on domain size. In c-Si, the phase transition pathway shifts from Si-I → Si-II in bulk Si to Si-I →Si-XI or Si-I →Si-V in nanostructured Si as domain size decreases [20]. Meanwhile, the critical transition pressure increases with decreasing domain size, rising from ~12 GPa in bulk Si to 17–22 GPa in SiNPs with sizes around or below 10 nm [20,21,23–25]. The elevated transition pressure in SiNPs has been attributed either to a lower density of defect nucleation sites for phase transitions or to a higher energy barrier for the Si-I → Si-II transition [20,21]. It should be noted that, the pressure-transmitting medium helium used in our high-pressure XRD experiment can provide nearly-hydrostatic conditions, therefore, the effect of shear stress on phase transitions is minimized.

To clarify the differences between a-Si and c-Si, we compared the pressure-induced phase transitions in a-SiNPs and crystalline SiNPs of the same particle size (~ 9 nm). The a-SiNPs transform into Si-II at 10.8 GPa, whereas crystalline SiNPs transform into Si-V at 16.4 GPa [20]. This comparison suggests that the phase transition pressure in a-SiNPs is significantly lower than that in crystalline SiNPs. One possible explanation is that the a-Si contains numerous intrinsic defects that act as nucleation sites for phase transitions, whereas such defects are typically scarce in c-Si. Another possible factor is that a-Si has a higher free energy than c-Si, which leads to a lower energy barrier for phase transition in a-Si. Further studies using techniques such as X-ray photon correlation spectroscopy can provide atomic-scale dynamics near phase transition [31,32]. It should be noted that a weak amorphous signal persists after the a-Si-to-Si-II transition (*e.g.*, at 18.3 and 21.7 GPa), which is most likely from the ultrathin native amorphous oxide layer (a-SiO_2) that naturally forms on Si surface upon air exposure, typically up to ~2 nm thick in bulk Si [33]. This assignment is supported by the match between the weak amorphous diffraction peak positions both at ambient pressure (Fig. S2) and at high pressures (*e.g.*, ~2.11 $Å^{-1}$ at ~21.7 GPa) with those of SiO_2 [17,34,35]. Since all forms of Si inherently possess a native oxide layer, the potential influence of this oxide layer on phase transitions should be similar across SiNPs, a-SiNPs, and other nanostructured Si. The mechanical confinement effect of such a thin a-SiO_2 layer is expected to be minor under high pressures, as the applied external pressure far exceeds the strength of the oxide. In addition, the interface between oxide layer and Si may serve as heterogenous nucleation sites for phase transitions. The effect of the native oxide layer on phase transitions will be an interesting topic to be addressed in the future.

In summary, we synthesized ~9 nm a-SiNPs and investigated their phase transitions under pressure using *in situ* high-pressure synchrotron XRD and Raman spectroscopy. The results suggest that the a-SiNPs transform into Si-II phase at ~10.8 GPa, rather than into a high-density amorphous phase. Upon further compression, the Si-II transforms to Si-XI at ~18.3 GPa, and subsequently to Si-V at ~21.7 GPa. Upon decompression, the Si-II phase reverts to a-Si. The phase transition pathway and transition pressure of the a-SiNPs are quite similar to their bulk counterpart, indicating the phase transition behavior in a-Si is much less sensitive to domain size than in c-Si. This may be attributed to the higher free energy state of a-Si relative to c-Si, or the presence of numerous defects in a-Si, both of which reduce the energy barrier for phase transitions. These results deepen our understanding of the thermodynamics and kinetics of phase transitions in a-Si and provide experimental constraints for theoretical studies of a-Si.

Data availability

The data that support the findings of this study are available from the corresponding author upon reasonable request.

CRediT authorship contribution statement

Haotian Zhu: Writing – original draft, Investigation. **Shuai Liu:** Writing – review & editing, Investigation. **Di Peng:** Writing – review & editing, Investigation. **Fujun Lan:** Writing – review & editing,

Investigation. **Yuxin Liu:** Writing – review & editing, Investigation. **Guangrun Zhong:** Writing – review & editing, Investigation. **Hongbo Lou:** Writing – review & editing, Investigation. **Qiaoshi Zeng:** Writing – review & editing, Supervision, Project administration, Funding acquisition. **Zhidan Zeng:** Writing – review & editing, Supervision, Conceptualization.

Declaration of competing interest

The authors declare that they have no known competing financial interests or personal relationships that could have appeared to influence the work reported in this paper.

Acknowledgments

The authors thank Drs. Shuai Yan and Lili Zhang for help in high-pressure synchrotron XRD experiments. The authors acknowledge the financial support from Shanghai Science and Technology Committee, China (No. 22JC1410300) and Shanghai Key Laboratory of Material Frontiers Research in Extreme Environments, China (No. 22dz2260800). We thank the Shanghai Synchrotron Radiation Facility of BL15U1 (https://cstr.cn/31124.02.SSRF.BL15U1) for the assistance on high-pressure XRD measurements.

Supplementary materials

Supplementary material associated with this article can be found, in the online version, at doi:10.1016/j.scriptamat.2025.117106.

References

[1] R. Street, Technology and applications of amorphous silicon, Springer Sc. Bus. Media (1999).
[2] B. Rech, H. Wagner, Potential of amorphous silicon for solar cells, Appl Phys A 69 (1999) 155–167.
[3] M.M.J. Treacy, K.B. Borisenko, The local structure of amorphous silicon, Science 335 (2012) 950–953.
[4] L.A.M. Rosset, D.A. Drabold, V.L. Deringer, Signatures of paracrystallinity in amorphous silicon from machine-learning-driven molecular dynamics, Nat. Commun. 16 (2025) 2360.
[5] R.C. Chittick, J.H. Alexander, H.F. Sterling, The preparation and properties of amorphous silicon, J. Electrochem. Soc. 116 (1969) 77.
[6] P.F. McMillan, M. Wilson, D. Daisenberger, D. Machon, A density-driven phase transition between semiconducting and metallic polyamorphs of silicon, Nat. Mater. 4 (2005) 680–684.
[7] S.K. Deb, M. Wilding, M. Somayazulu, P.F. McMillan, Pressure-induced amorphization and an amorphous–amorphous transition in densified porous silicon, Nature 414 (2001) 528–530.
[8] D. Daisenberger, T. Deschamps, B. Champagnon, M. Mezouar, R.Quesada Cabrera, M. Wilson, P.F. McMillan, Polyamorphic amorphous silicon at high pressure: raman and spatially R esolved X-ray scattering and molecular dynamics studies, J. Phys. Chem. B 115 (2011) 14246–14255.
[9] V.L. Deringer, N. Bernstein, G. Csányi, C. Ben Mahmoud, M. Ceriotti, M. Wilson, D. A. Drabold, S.R. Elliott, Origins of structural and electronic transitions in disordered silicon, Nature 589 (2021) 59–64.
[10] T. Morishita, High density amorphous form and polyamorphic transformations of silicon, Phys. Rev. Lett. 93 (2004) 055503.
[11] Z. Fan, H. Tanaka, Microscopic mechanisms of pressure-induced amorphous-amorphous transit ions and crystallisation in silicon, Nat. Commun. 15 (2024) 368.
[12] M. Imai, T. Mitamura, K. Yaoita, K. Tsuji, Pressure-induced phase transition of crystalline and amorphous silicon and germanium at low temperatures, Res 15 (1996) 167–189.
[13] D. Daisenberger, M. Wilson, P.F. McMillan, R.Quesada Cabrera, M.C. Wilding, D. Machon, High-pressure x-ray scattering and computer simulation studies of density-induced polyamorphism in silicon, Phys. Rev. B 75 (2007) 224118.
[14] B. Haberl, M. Guthrie, David J. Sprouster, Jim S. Williams, Jodie E. Bradby, New insight into pressure-induced phase transitions of amorphous silicon: the role of impurities, J. Appl. Crystallogr. 46 (2013) 758–768.
[15] N. Garg, K.K. Pandey, K.V. Shanavas, C.A. Betty, S.M. Sharma, Memory effect in low-density amorphous silicon under pressure, Phys. Rev. B 83 (2011) 115202.
[16] K.K. Pandey, N. Garg, K.V. Shanavas, S.M. Sharma, S.K. Sikka, Pressure induced crystallization in amorphous silicon, J. Appl. Phys. 109 (2011) 113511.
[17] C. Lin, X. Liu, D. Yang, X. Li, J.S. Smith, B. Wang, H. Dong, S. Li, W. Yang, J.S. Tse, Temperature- and rate-dependent pathways in formation of metastable silicon phases under rapid decompression, Phys. Rev. Lett. 125 (2020) 155702.
[18] J.Z. Hu, L.D. Merkle, C.S. Menoni, I.L. Spain, Crystal data for high-pressure phases of silicon, Phys. Rev. B 34 (1986) 4679–4684.
[19] Z. Zeng, Q. Zeng, M. Ge, B. Chen, H. Lou, X. Chen, J. Yan, W. Yang, H.-K. Mao, D. Yang, W.L. Mao, Origin of plasticity in nanostructured silicon, Phys. Rev. Lett. 124 (2020) 185701.
[20] Y. Xuan, L. Tan, B. Cheng, F. Zhang, X. Chen, M. Ge, Q. Zeng, Z. Zeng, Pressure-induced phase transitions in nanostructured silicon, J. Phys. Chem. C 124 (2020) 27089–27096.
[21] S.H. Tolbert, A.B. Herhold, L.E. Brus, A.P. Alivisatos, Pressure-induced structural transformations in Si nanocrystals: surface and shape effects, Phys. Rev. Lett. 76 (1996) 4384–4387.
[22] L.Q. Huston, A. Lugstein, J.S. Williams, J.E. Bradby, The high pressure phase transformation behavior of silicon nanowires, Appl. Phys. Lett. 113 (2018) 123103.
[23] D.C. Hannah, J. Yang, P. Podsiadlo, M.K.Y. Chan, A. Demortière, D.J. Gosztola, V. B. Prakapenka, G.C. Schatz, U. Kortshagen, R.D. Schaller, On the origin of photoluminescence in silicon nanocrystals: pressure-D ependent structural and optical studies, Nano Lett. 12 (2012) 4200–4205.
[24] N.N. Ovsyuk, S.G. Lyapin, Raman spectra of Si nanocrystals under high pressure: metallization and solid state amorphization, Appl. Phys. Lett. 116 (2020) 062103.
[25] R.A. Senter, C. Pantea, Y. Wang, H. Liu, T.W. Zerda, J.L. Coffer, Structural influence of erbium centers on silicon nanocrystal phase transitions, Phys. Rev. Lett. 93 (2004) 175502.
[26] O.L. Anderson, D.G. Isaak, S. Yamamoto, Anharmonicity and the equation of state for gold, J. Appl. Phys. 65 (1989) 1534–1543.
[27] C. Prescher, V.B. Prakapenka, DIOPTAS: a program for reduction of two-dimensional X-ray diffraction data and data exploration, High Press, Res 35 (2015) 223–230.
[28] R.W. Cahn, Metallic solid silicon, Nature 357 (1992) 645–646.
[29] X. Zhang, X. Wang, Z. Zhang, W. Shen, C. Fang, L. Chen, Y. Zhang, B. Wan, Q. Wang, J. He, Y. Pan, Phase evolution of bulk nanocrystalline silicon At high pressure, J. Phys. Chem. C 128 (2024) 14842–14848.
[30] R.H. Klazes, M.H.L.M. van den Broek, J. Bezemer, S.J.P.M. Radelaar, Determination of the optical bandgap of amorphous silicon, Philos. Mag. B 45 (1982) 377–383.
[31] Q. Zeng, In situ high-pressure wide-angle hard x-ray photon correlation spectroscopy: a versatile tool probing atomic dynamics of extreme condition matter, Matter Radiat. Extrem. 8 (2023) 028101.
[32] X. Zhang, H. Lou, B. Ruta, Y. Chushkin, F. Zontone, S. Li, D. Xu, T. Liang, Z. Zeng, H.-K. Mao, Q. Zeng, Pressure-induced nonmonotonic cross-over of steady relaxation dynamics in a metallic glass, Proc. Natl. Acad. Sci. U.S.A. 120 (2023) e2302281120.
[33] M. Morita, T. Ohmi, E. Hasegawa, M. Kawakami, M. Ohwada, Growth of native oxide on a silicon surface, J. Appl. Phys. 68 (1990) 1272–1281.
[34] G. Shen, Q. Mei, V.B. Prakapenka, P. Lazor, S. Sinogeikin, Y. Meng, C. Park, Effect of helium on structure and compression behavior of SiO_2 glass, Nat. Commun. 108 (2011) 6004–6007.
[35] W. Jin, R.K. Kalia, P. Vashishta, J.P. Rino, Structural transformation in densified silica glass: a molecular-dynamics study, Phys. Rev. B 50 (1994) 118–131.